Atmospheric Circulation and Tides of "51 Peg b-like" Planets

Adam P. Showman[1] **and Tristan Guillot**[2]

[1] University of Arizona, Department of Planetary Sciences and Lunar and Planetary Laboratory, Tucson, AZ 85721; showman@lpl.arizona.edu

[2] Observatoire de la Côte d'Azur, Laboratoire Cassini, CNRS UMR 6529, 06304 Nice Cedex 4, France; guillot@obs-nice.fr

Abstract. We examine the properties of the atmospheres of extrasolar giant planets at orbital distances smaller than 0.1 AU from their stars. We show that these "51 Peg b-like" planets are rapidly synchronized by tidal interactions, but that small departures from synchronous rotation can occur because of fluid-dynamical torques within these planets. Previous radiative-transfer and evolution models of such planets assume a homogeneous atmosphere. Nevertheless, we show using simple arguments that, at the photosphere, the day-night temperature difference and characteristic wind speeds may reach ~ 500 K and ~ 2 km sec^{-1}, respectively. Substantial departures from chemical equilibrium are expected. The cloud coverage depends sensitively on the dynamics; clouds could exist predominantly either on the dayside or nightside, depending on the circulation regime. Radiative-transfer models that assume homogeneous conditions are therefore inadequate in describing the atmospheric properties of 51 Peg b-like planets. We present preliminary three-dimensional, nonlinear simulations of the atmospheric circulation of HD209458b that indicate plausible patterns for the circulation and generally agree with our simpler estimates. Furthermore, we show that kinetic energy production in the atmosphere can lead to the deposition of substantial energy in the interior, with crucial consequences for the evolution of these planets. Future measurements of reflected and thermally-emitted radiation from these planets will help test our ideas.

Key words: extrasolar planets, 51 Peg, HD209458, tides, atmospheric dynamics, interior structure, giant planets

1. Introduction

The discovery of extrasolar planets has led to a growing list of work devoted to modeling their atmospheres (Burrows et al. 1997; Seager and Sasselov 1998, 2000; Goukenleuque et al. 2000; Barman et al. 2001). While no spectra of these objects have yet been measured, one might be encouraged by the successes obtained in the case of the similar brown dwarfs, for which theoretical models now reproduce the observations well, even in the case of low-temperature objects ($T_{\rm eff} \sim 1000$ K or less) (e.g. Marley et al. 1996; Allard et al. 1997; Liebert et al. 2000; Geballe et al. 2001; Schweitzer et al. 2001 to cite only a few). However, an important feature of extrasolar planets is their proximity to a star: The irradiation that they endure can make their atmospheres significantly different than those of isolated brown dwarfs with the same effective temperature. This has been shown to profoundly alter the atmospheric vertical temperature profile (Seager and Sasselov 1998; Goukenleuque et al. 2000; Barman et al. 2001). We will show that most importantly, it also affects the horizontal temperature distribution and atmospheric chemistry so that the models calculated thus far may fail to provide an adequate description of the atmospheres of the most intensely irradiated planets. Advection has never previously been considered, but it can play a major role for the composition, temperature, spectral appearance and evolution of extrasolar planets.

We will focus on the extrasolar planets for which irradiation is the most important: 51 Peg b-like planets, which we henceforth dub "Pegasi planets" and define as gas giants orbiting solar-type stars at less than 0.1 AU. Their importance is demonstrated by the fact that they orbit nearly 1% of stars surveyed so far and constitute 27% of currently-known extrasolar giant planets. They are also more easily characterized by the transit method than are other planets, as indicated by the discovery of the transiting gas giant HD209458b (Charbonneau et al. 2000; Henry et al. 2000). In the preceeding paper (Guillot and Showman 2001, hereafter Paper I), we showed how the atmospheric boundary condition governs the evolution of Pegasi planets. We also advocated that an additional source of energy is needed to explain the radius HD209458b, and that this would most likely be provided by the downward transport and subsequent dissipation of kinetic energy with a flux of $\sim 1\%$ of the absorbed stellar energy. In this paper, we use the temperature profiles obtained in Paper I to evaluate the dynamical state of Pegasi-planet atmospheres, and discuss how dynamics may in-

fluence the cloud abundance, chemical composition, and thermal state (all of which will be amenable to observation in the near future). We then present preliminary numerical simulations of the circulation that indicate plausible circulation patterns and show how downward propagation of kinetic energy from the atmosphere to the interior can occur.

After reviewing the expected interior structure (Section 2), we begin in Section 3 with the problem of tides: Pegasi planets have been predicted to rotate synchronously (Guillot et al. 1996), implying that they always present the same face toward the star. We argue however that dynamical torques may maintain the interior in a non-synchronous rotation state, which has important implications for understanding atmospheric processes. In section 4, we discuss the probable wind speeds, day-night temperature differences, and flow geometries, including both order-of-magnitude arguments and our numerical simulations. A summary of the results is provided in section 5.

2. Interior structure

Fully self-consistent models including both the atmospheres and interiors of Pegasi planets do not yet exist. To obtain first-cut estimates of the expected temperature profiles, we therefore use the same approach as in Paper I: we choose two extreme evolution models ("hot" and "cold") that match the radius of HD209458b (but at different ages and hence intrinsic luminosities). These evolution calculations only pertain to pressures larger than 3 to 10 bars (depending on the boundary condition), and so we extend the profiles to lower pressure using radiative-transfer calculations for intensely-irradiated planets from Marley (personal communication) and Barman (2001). The calculations are not strictly appropriate to the case of HD209458b, but provide us with reasonable estimates of the expected structure (and as we will see our qualitative conclusions are not sensitive to the type of profile chosen). The resulting "hot" and "cold" models that we will use hereafter are depicted in Figure 1. Interestingly, Paper I shows that these two models are representative of a relatively wide variety of models of HD209458b, including those with energy dissipation.

It should be noted that the high temperatures can trigger the dissociation of the hydrogen molecule, which is indicated in Fig. 1 by a local maximum of the heat capacity c_p. This effect is important for our purposes because it implies that stellar heat can be stored in hot regions and reclaimed in colder regions by molecular recombination. Other molecules (e.g. H_2O) can undergo dissociation, but this will be neglected due to their small abundances.

Evolution models of Pegasi planets show that two interior regions exist: a radiative zone (including the atmosphere) that extends down to pressures of 100 to 800 bar, and a deeper convective core. The intrinsic luminosity of
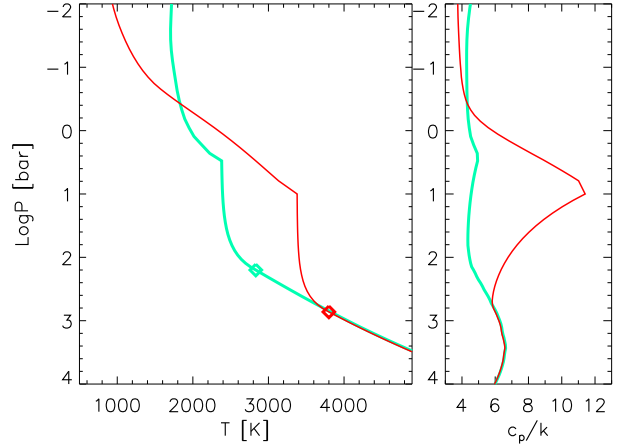

Fig. 1. *Left:* Temperature profiles for the "hot" model (thin line) and "cold" model (thick grey line) at times (5.37 and 0.18 Ga, respectively) when the models match HD209458b's measured radius. The diamonds indicate the radiative/convective boundary. The terms "hot" and "cold" are chosen to indicate the models' relative temperatures in the region from ∼ 1–300 bars, which is the important region of the atmosphere for affecting the evolution. See Paper I for details. The discontinuity in the profiles' slopes is unphysical; it results from the fact that atmospheric models assume a much higher intrinsic luminosity than predicted by evolution models. *Right:* Dimensionless mean specific heat per particle in the atmosphere. The local maxima in c_p are due to the dissociation of the H_2 molecule.

the planet is about 10,000 times smaller than the energy absorbed from the star. If energy dissipation in the outer layers is large (see Paper I), another convective zone can appear at the levels where dissipation is the largest. This however requires a very high dissipation of ∼ 10% of the incoming heat flux. We therefore chose to only consider the simple radiative/convective scenario, as depicted in Fig. 2.

We split the planet into an "atmosphere" dominated by stellar heating, with possible horizontal temperature inhomogeneities, and an "interior" including the convective core, for which inhomogeneities should be much smaller. The crux of the problem is to understand how the heat absorbed on the day side and near the equator is redistributed by winds and/or rotation to the night side and to the poles.

3. Synchronization of Pegasi planets

It has been shown that the tides raised by the star on Pegasi planets should rapidly drive them into synchronous rotation (Guillot et al. 1996; Marcy et al. 1997; Lubow et al. 1997). This can be seen by considering the time
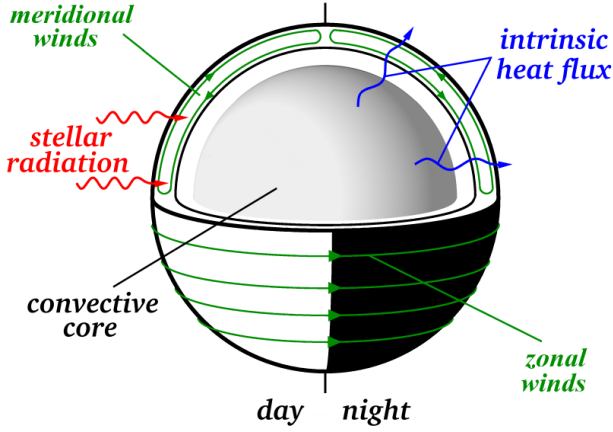
Fig. 2. Conjectured dynamical structure of Pegasi planets: At pressures larger than 100–800 bar, the intrinsic heat flux must be transported by convection. The convective core is at or near synchronous rotation with the star and has small latitudinal and longitudinal temperature variations. At lower pressures a radiative envelope is present. The top part of the atmosphere is penetrated by the stellar light on the day side. The spatial variation in insolation should drive winds that transport heat from the day side to the night side (see text).

scale to tidally despin the planet (Goldreich & Soter 1966; Hubbard 1984):

$$\tau_{\rm syn} \approx Q\left(\frac{R^3}{GM}\right)(\omega - \omega_{\rm s})\left(\frac{M}{M_\star}\right)^2\left(\frac{a}{R}\right)^6, \tag{1}$$

where Q, R, M, a, ω and $\omega_{\rm s}$ are the planet's tidal dissipation factor, radius, mass, orbital semi-major axis, rotational angular velocity, and synchronous (or orbital) angular velocity. M_* is the star's mass, and G is the gravitational constant. Factors of order unity have been omitted. A numerical estimate for HD209458b (with ω equal to the current Jovian rotation rate) yields a spindown time $\tau_{\rm syn} \sim 3Q$ years. Any reasonable dissipation factor Q (see Marcy et al. 1997; Lubow et al. 1997) shows that HD209458b should be led to synchronous rotation in less than a few million years, i.e., on a time scale much shorter than the evolution timescale. Like other Pegasi planets, HD209458b is therefore expected to be in synchronous rotation with its 3.5-day orbital period.

Nevertheless, stellar heating drives the atmosphere away from synchronous rotation, raising the possibility that the interior's rotation state is not fully synchronous. Here, we discuss (1) the energies associated with the planet's initial transient spindown, and (2) the possible equilibrium states that could exist at present.

3.1. Spindown energies

Angular momentum conservation requires that as the planet spins down, the orbit expands. The energy dissipated during the spindown process is the difference between the loss in spin kinetic energy and the gain in orbital energy:

$$\dot{E} = -\frac{d}{dt}\left(\frac{1}{2}k^2MR^2\omega^2 - \frac{1}{2}Ma^2\omega_{\rm s}^2\right), \tag{2}$$

where k is the dimensionless radius of gyration ($k^2 = I/MR^2$, I being the planet's moment of inertia). The time derivative is negative, so $\dot{E}$, the energy dissipated, is positive. The orbital energy is the sum of the planet's gravitational potential energy and orbital kinetic energy and is negative by convention. The conservation of angular momentum implies that the rate of change of $\omega_{\rm s}$ is constrained by that on ω:

$$\frac{d}{dt}\left(Ma^2\omega_{\rm s} + k^2MR^2\omega\right) = 0. \tag{3}$$

The fact that the planetary radius changes with time may slightly affect the quantitative results. However, since $\tau_{\rm syn}$ is so short, it can be safely neglected in this first-order estimate. R being held constant, it is straightforward to show, using Kepler's third law, that:

$$\dot{E} = -k^2MR^2(\omega - \omega_{\rm s})\dot{\omega}. \tag{4}$$

(Note that $\dot{\omega}$ is negative, and so $\dot{E}$ is positive.)

The total energy dissipated is $E \approx k^2MR^2(\omega_{\rm s}-\omega)^2/2$, neglecting variation of the orbital distance. Using the moment of inertia and rotation rate of Jupiter ($k^2 = 0.26$ and $\omega = 1.74 \times 10^{-4}$ sec^{-1}), we obtain for HD209458b $E \approx 4 \times 10^{41}$ erg. If this energy were dissipated evenly throughout the planet, it would imply a global temperature increase of 1400 K.

By definition of the synchronization timescale, the dissipation rate can be written:

$$\dot{E} = \frac{k^2MR^2(\omega - \omega_{\rm s})^2}{\tau_{\rm syn}}. \tag{5}$$

With Q of 10^5, a value commonly used for Jupiter, $\tau_{\rm syn} \sim 3 \times 10^5$ years and the dissipation rate is then $\sim 10^{29}$ erg sec^{-1}, or 35,000 times Jupiter's intrinsic luminosity. Lubow et al. (1997) have suggested that dissipation in the radiative zone could exceed this value by up to two orders of magnitude, but this would last for only ~ 100 years.

The thermal pulse associated with the initial spindown is large enough that, if the energy is dissipated in the planet's interior, it may affect the planet's radius. It has previously been argued (Burrows et al. 2000) that Pegasi planets must have migrated inward during their first 10^7 years of evolution; otherwise, they would have contracted too much to explain the observed radius of

HD209458b. But the thermal pulse associated with spin-down was not included in the calculation, and this extra energy source may extend the time over which migration was possible.

Nevertheless, it seems difficult to invoke tidal synchronization as the missing heat source necessary to explain HD209458b's present (large) radius. High dissipation rates are possible if $\tau_{\rm syn}$ is small, but in the absence of a mechanism to prevent synchronization, $\dot{E}$ would drop as soon as $t > \tau_{\rm syn}$. The most efficient way of slowing the planet's contraction is then to invoke $\tau_{\rm syn} \sim 10^{10}$ years. In that case, the energy dissipated becomes $\dot{E} \sim 10^{24}\,{\rm erg\,sec^{-1}}$, which is two orders of magnitude smaller than that necessary to significantly affect the planet's evolution (Paper I; Bodenheimer et al. 2001). For the present-day dissipation to be significant, an initial rotation rate 10 times that of modern-day Jupiter would be needed. But the centripetal acceleration due to rotation exceeds the gravitational acceleration at the planet's surface for rotation rates only twice that of modern-day Jupiter, so this possibility is ruled out. Furthermore, such long spindown times would require a tidal Q of $\sim 10^{9}$–10^{10}, which is $\sim 10^{4}$ times the Q values inferred for Jupiter, Uranus, and Neptune from constraints on their satellites' orbits (Peale 1999, Banfield and Murray 1992, Tittemore and Wisdom 1989). Dissipation of the energy due to transient loss of the planet's initial spin energy therefore cannot provide the energy needed to explain the radius of HD209458b.

Another possible source of energy is through circularization of the orbit. Bodenheimer et al. (2001) show that the resulting energy dissipation could reach $10^{26}\,{\rm erg\,sec^{-1}}$ if the planet's tidal Q is 10^{6} and if a hypothetical companion planet pumps HD209458b's eccentricity to values near its current observational upper limit of 0.04. If such a companion is absent, however, the orbital circularization time is $\sim 10^{8}$ years, so this source of heating would be negligible at present. Longer circularization times of 10^{9}–10^{10} years would allow the heating to occur until the present-day, but its magnitude is then reduced to $10^{25}\,{\rm erg\,sec^{-1}}$ or lower, which is an order of magnitude smaller than the dissipation required.

3.2. The equilibrium state

The existence of atmospheric winds implies that the atmosphere is not synchronously rotating. Because dynamics can transport angular momentum vertically and horizontally (including the possibility of downward transport into the interior), the interior may evolve to an equilibrium rotation state that is asynchronous. Here we examine the possibilities.

Let us split the planet into an "atmosphere", a part of small mass for which thermal effects are significant, and an "interior" encompassing most of the mass which has minimal horizontal thermal contrasts. Suppose (since $\tau_{\rm syn}$ is short) that the system has reached steady state. Consider

two cases, depending on the physical mechanisms that determine the gravitational torque on the atmosphere.

The first possibility is that the gravitational torque on the atmosphere pushes the atmosphere away from synchronous rotation (i.e., it increases the magnitude of the atmosphere's angular momentum measured in the synchronously-rotating reference frame) as has been hypothesized for Venus (Ingersoll and Dobrovolskis 1978, Gold and Soter 1969). To balance the torque on the atmosphere, the interior must have a net angular momentum of the same sign as the atmosphere (so that both either super- or subrotate). In Fig. 3, superrotation then corresponds to a clockwise flux of angular momentum, whereas subrotation corresponds to the anticlockwise scenario.

The second possibility is that the gravitational torque on the atmosphere tends to synchronize the atmosphere. This possibility may be relevant because, on a gas-giant planet, it is unclear that the high-temperature and high-pressure regions would be 90° out of phase, as is expected on a terrestrial planet. If the interior responds sufficiently to atmospheric perturbations to keep the deep isobars independent of surface meteorology (an assumption that seems to work well in modeling Jupiter's cloud-layer dynamics), then high-pressure and high-temperature regions will be *in* phase, which would sweep the high-mass regions downwind and lead to a torque that synchronizes the atmosphere. Furthermore, if a resonance occurs between the tidal frequency and the atmosphere's wave-oscillation frequency, the resulting gravitational torques also act to synchronize the atmosphere (Lubow et al. 1997). In this case, the interior and atmosphere have net angular momenta of opposite signs. Depending on the sign of the atmosphere/interior momentum flux, this situation would correspond in Fig. 3 to either the clockwise or anticlockwise circulation of angular momentum cases.

In both cases above, the gravitational torque on the atmosphere arises because of spatial density variations associated with surface meteorology, which are probably confined to pressures less than few hundred bars. Therefore, this torque acts on only a small fraction of the planet's mass. In contrast, the gravitational torque on the gravitational tidal bulge affects a much larger fraction of the planet's mass. It is not necessarily true that the torque on the atmosphere is negligible in comparison with the torque on the interior, however, because the gravitational tidal bulge is only slightly out of phase with the line-of-sight to the star (e.g., the angle is 10^{-5} radians for Jupiter). In contrast, the angle between the meteorologically-induced density variations and the line of sight to the star could be up to a radian. Detailed calculations of torque magnitudes would be poorly constrained, however, and will be left for the future.

Several mechanisms may act to transfer angular momentum between the atmosphere and interior. Kelvin-Helmholtz shear instabilities, if present, would smooth interior-atmosphere differential rotation. On the other
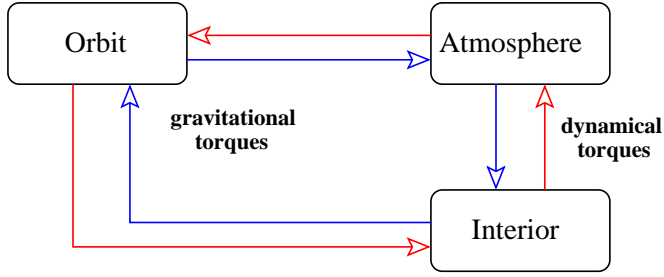
Fig. 3. Angular momentum flow between orbit, interior, and atmosphere for a Pegasi planet in steady state. Arrows indicate flow of prograde angular momentum (i.e., that with the same sign as the orbital angular momentum) for two cases: *Anticlockwise:* Gravitational torque on atmosphere is retrograde (i.e., adds westward angular momentum to atmosphere). For torque balance, the gravitational torque on the interior must be prograde (i.e., eastward). These gravitational torques must be balanced by fluid-dynamical torques that transport retrograde angular momentum from atmosphere to interior. *Clockwise:* Gravitational torque on atmosphere is prograde, implying a retrograde torque on the interior and downward transport of prograde angular momentum from atmosphere to interior. Atmosphere will superrotate if gravitational torques push atmosphere away from synchronous (as on Venus). It will subrotate if gravitational torques synchronize the atmosphere (e.g., gravity-wave resonance; cf. Lubow et al. (1997)).

hand, waves transport angular momentum and, because they act nonlocally, often *induce* differential rotation rather than removing it. The quasi-biennial oscillation on Earth is a classic example (see, e.g., Andrews et al. 1987, Chapter 8). Atmospheric tides (large-scale waves forced by the solar heating) are another example of such a wave; on Venus, tides play a key role in increasing the rotation rate of the cloud-level winds. Finally, vertical advection may cause angular momentum exchange between the atmosphere and the interior of Pegasi planets, because the angular momentum of air in updrafts and downdrafts need not be the same.

A simple estimate illustrates the extent of nonsynchronous rotation possible in the interior. Suppose that the globally-averaged flux of absorbed starlight is $F_\odot$, which is of order $10^8 \, \mathrm{erg \, s^{-1} \, cm^{-2}}$ for Pegasi planets near 0.05 AU, and that the globally-averaged flux of kinetic energy transported from the atmosphere to the interior is $\eta F_\odot$, where η is small and dimensionless. If this kinetic energy flux is balanced by dissipation in the interior with a spindown timescale of τ_{syn}, then the deviation of the rotation frequency from synchronous is

$$\omega - \omega_s = \left(\frac{4\pi \eta F_\odot \tau_{\mathrm{syn}}}{k^2 M} \right)^{1/2} \qquad (6)$$

This estimate is an upper limit for the *globally averaged* asynchronous rotation rate because it assumes that kinetic energy transported into the interior has angular momentum of a single sign. The global-average asynchronous rotation could be even lower if angular momenta transported downward in different regions have opposite signs.

The spindown time is uncertain and depends on the planet's Q according to Eq. (1). To date, only one estimate for the Q of a Pegasi planet exists (Lubow et al. 1997), which suggests $Q \sim 100$, at least during the early stages of spindown. Orbital constraints on the natural satellites of the giant planets imply that, at periods of a few days, the tidal Q of Uranus, Neptune, and Jupiter are of order $\sim 10^5$ (Tittemore and Wisdom 1989, Banfield and Murray 1992, Peale 1999), which suggests a spindown time of a few $\times 10^5$ years (Eq. 1). Although the mechanisms that determine these planets' Q values remain uncertain, likely possibilities include friction in the solid inner core (Dermott 1979) or overturning of tidally-forced waves in the fluid envelope (Ioannou and Lindzen 1993, Houben et al. 2001). Both mechanisms are possible for Pegasi planets, and the wave-dissipative mechanism should be more effective for Pegasi planets than for Jupiter because of the thicker stable (radiative) layer in the former (Houben et al. 2001). These calculations suggest that spindown times of $\sim 10^5$–10^6 years are likely, although larger values cannot be ruled out.

As discussed in Section 4, experience with planets in our solar system suggests that atmospheric kinetic energy is generated at a flux of $10^{-2} F_\odot$, and if all of this energy enters the interior, then $\eta \sim 10^{-2}$. Using a spindown time of 3×10^5 years implies that $\omega - \omega_s \sim 2 \times 10^{-5} \, \mathrm{sec^{-1}}$, which is comparable to the synchronous rotation frequency. The implied winds in the interior are then of order $\sim 2000 \, \mathrm{m \, sec^{-1}}$. Even if η is only 10^{-4}, the interior's winds would be $200 \, \mathrm{m \, sec^{-1}}$. The implication is that the interior's spin could be asynchronous by up to a factor of two, depending on the efficiency of energy and momentum transport into the interior. If spindown times of $\sim 10^6$ years turn out to be serious under- or overestimates, then greater or lesser asynchronous rotation would occur, respectively.

4. Atmospheric Circulation: Possible regimes and influence on evolution

4.1. Basic Parameter Regime

Rotation plays a central role in the atmospheric dynamics of Pegasi planets, and HD209458b in particular. The ratio of nonlinear advective accelerations to Coriolis accelerations in the horizontal momentum equation is $u f^{-1} L^{-1}$ (called the Rossby number), where u is the mean horizontal wind speed, $f = 2\Omega \sin\phi$ is the "Coriolis parameter" (e.g. Holton 1992, pp. 39-40), Ω is the rotational angular velocity, ϕ is latitude, and L is a characteristic

length scale. Rossby numbers of 0.03–0.3 are expected for winds of planetary-scale and speeds ranging from 100–1000 m sec^{-1}. In Section 3 we showed that modest asynchronous rotation may occur, in which case the Rossby number could differ from this estimate by a factor up to ~ 2. These estimates suggest that nonlinear advective terms are small compared to the Coriolis accelerations, which must then balance with the pressure-gradient accelerations. (The Rossby number could be ~ 1 if the winds reach 2000–3000 m sec^{-1}, which we show below is probably the maximum allowable wind speed.)

The zonality of the flow can be characterized by the Rhines' wavenumber, $k_\beta \sim (\beta/u)^{1/2}$, where β is the derivative of f with northward distance (Rhines 1975). The half-wavelength implied by this wavenumber, called the Rhines' scale L_β, provides a reasonable estimate for the jet widths on all four outer planets in our solar system (Cho and Polvani 1996; see Table 1). For HD209458b, the Rhines' scale is $\sim 1.5 \times 10^{10}(u/1000\,\mathrm{m\,sec}^{-1})^{1/2}$ cm, which exceeds the planetary radius if the wind speed exceeds about 400 m sec^{-1}.

Another measure of horizontal structure is the Rossby deformation radius (Gill 1982, p. 205), $L_D \sim NH/f$, where H is the scale height and N is the Brünt-Vaisala frequency (i.e., the oscillation frequency for a vertically displaced air parcel; Holton 1992, p. 54). At pressures of a few bars, the temperature profiles calculated for irradiated extrasolar giant planets by Goukenlouque et al. (2000) suggest $N \sim 0.0015\,\mathrm{sec}^{-1}$. With a scale height of 700 km, the resulting deformation radius is 40,000 km. In contrast, the deformation radii near the tropopause of the Jupiter, Saturn, Uranus, and Neptune are of order 2000 km (Table 1).

The estimated Rhines' scale (for winds of $>$ 500 m sec^{-1}, which we show later are plausible speeds) and deformation radius of Pegasi planets are similar to the planetary radius, and they are a larger fraction of the planetary radius than is the case for Jupiter, Saturn, Uranus, and Neptune (Table 1). This fact suggests that eddies may grow to hemispheric scale in the atmospheres of Pegasi planets and that, compared with the giant planets in our solar system, the general circulation hot Jupiters may be more global in character. Unless the winds are extremely weak, Pegasi planets are unlikely to have > 10 jets as do Jupiter and Saturn.

An upper limit on the atmospheric wind speed can be derived from shear-instability considerations. We assume that no zonal winds are present ($u(P_0) = 0$) in the convective core, a consequence of synchronization by tidal friction. The build-up of winds at higher altitudes in the radiative envelope is suppressed by Kelvin-Helmholtz instabilities if the shear becomes too large. This occurs when the Richardson number becomes smaller than 1/4 (cf. Chandrasekhar 1961), i.e. when

$$Ri = \frac{N^2}{(du/dz)^2} < \frac{1}{4}, \tag{7}$$

In the perfect gas approximation, assuming a uniform composition,

$$N^2 = \frac{g}{H}(\nabla_{\mathrm{ad}} - \nabla_T). \tag{8}$$

where $\mathcal{R}$ is the universal gas constant divided by the mean molecular mass, c_p is the specific heat, $H = \mathcal{R}T/g$ is the pressure scale height, $\nabla_{\mathrm{ad}} = \mathcal{R}/c_p$ is the adiabatic gradient, $\nabla_T = d\ln T/d\ln p$, T is temperature, and p is pressure. The hypothesis of uniform composition is adequate despite hydrogen dissociation because the timescales involved are generally much longer than the dissociation timescales. It can be noted that a shear instability could appear at smaller Richardson numbers in the presence of efficient radiative diffusion (Zahn 1992; Maeder 1995). This possibility will not be examined here.

The maximal wind speed at which Kelvin-Helmholtz instabilities occur can then be derived by integration of Eq. (7):

$$u_{\max}(P) \sim \frac{1}{2}\int_{P_0}^{P}[\mathcal{R}T(\nabla_{\mathrm{ad}} - \nabla_T)]^{1/2}\,d\ln p, \tag{9}$$

The value of $u_{\max}$ thus derived at $P \sim 1\,\mathrm{bar}$ is of the order of 3000 m s^{-1}, to be compared to the winds of Jupiter, Saturn, Uranus and Neptune which reach 100–500 m s^{-1} (Ingersoll et al. 1995). Our estimate for Pegasi planets, assuming the winds are measured in the synchronously-rotating frame, may be uncertain by a factor of ~ 2 due to the possibility of a non-synchronously-rotating interior. In comparison, the expected speed of sound at the tropopause of HD209458b is ~ 2400 m sec^{-1}.

A characteristic timescale for zonal winds to redistribute temperature variations over scales similar to the planetary radius R then stems from $\tau_{\mathrm{zonal}} \gtrsim R/u_{\max}$.

The radiative heating timescale can be estimated by a ratio between the thermal energy within a given layer and the layer's net radiated flux. In the absence of dynamics, absorbed solar fluxes balance the radiated flux, but dynamics perturbs the temperature profile away from radiative equilibrium. Suppose the radiative equilibrium temperature at a particular location is T_{rad} and the actual temperature is $T_{\mathrm{rad}} + \Delta T$. The net flux radiated towards outer space is then $4\sigma T_{\mathrm{rad}}^3\Delta T$ and the radiative timescale is

$$\tau_{\mathrm{rad}} \sim \frac{P}{g}\frac{c_p}{4\sigma T^3}, \tag{10}$$

where σ is the Stefan-Boltzmann constant.

Figure 4 shows estimates of τ_{zonal} and τ_{rad} for HD209458b calculated using the temperature profiles from the "hot" (thin line) and "cold" (thick grey line) models

Table 1. Rhines' and deformation lengths for giant planets

	u ($\mathrm{m\,sec^{-1}}$)	R ($10^7\,\mathrm{m}$)	Ω ($10^{-4}\,\mathrm{sec^{-1}}$)	L_β ($10^7\,\mathrm{m}$)	L_D ($10^7\,\mathrm{m}$)	Jet width ($10^7\,\mathrm{m}$)
Jupiter	50	7.1	1.74	1.0	0.2	~ 1
Saturn	200	6.0	1.6	1.9	0.2	~ 2
Uranus	300	2.6	1.0	2.0	0.2	~ 2
Netpune	300	2.5	1.1	1.9	0.2	~ 2
HD209458b	?	10	~ 0.2	$15(u/1\,\mathrm{km\,sec^{-1}})^{1/2}$	~ 4	?

Note. L_D calculated at the tropopause using $N = 0.01\,\mathrm{sec^{-1}}$ for Saturn, Uranus, and Neptune, and $N = 0.02\,\mathrm{sec^{-1}}$ for Jupiter.

from Section 2. The zonal timescale is estimated by calculating the maximum wind speed that can exist as a function of pressure given the static stability associated with each model, while the radiative time is calculated using the temperatures and heat capacities shown in Fig. 1. At pressures exceeding 0.1 bar, radiation is slower than the maximal advection by zonal winds, but by less than one order of magnitude. The consequent day/night temperature difference $\Delta T_{\mathrm{day-night}}$ to be expected is:

$$\frac{\Delta T_{\mathrm{day-night}}}{\Delta T_{\mathrm{rad}}} \sim 1 - e^{-\tau_{\mathrm{zonal}}/\tau_{\mathrm{rad}}}. \qquad (11)$$

where ΔT_{rad} is the day-night difference in radiative equilibrium temperatures. Rough estimates from Fig. 4 suggest that $\tau_{\mathrm{zonal}}/\tau_{\mathrm{rad}} \sim 0.3$ at 1 bar, implying that $\Delta T_{\mathrm{day-night}}/\Delta T_{\mathrm{rad}} \sim 0.3$. If $\Delta T_{\mathrm{rad}} = 1000\,\mathrm{K}$, this would imply day-night temperature differences of $300\,\mathrm{K}$ at 1 bar. Values of $\Delta T_{\mathrm{day-night}}$ even closer to ΔT_{rad} are likely given the fact that slower winds will lead to an even more effective cooling on the night side and heating on the day side.

The small radiative time scale implies that, for the day-night temperature difference to be negligible near the planet's photosphere, atmospheric winds would have to be larger than the maximum winds for the onset of shear instabilities.

4.2. Nature of the circulation

An understanding of the horizontal temperature difference and mean wind speed is desirable. It is furthermore of interest to clarify the possible geometries the flow may take. For Pegasi planets, we envision that the dominant forcing is the large-scale day-night heating contrast, with minimal role for moist convection. This situation differs from that of Jupiter, where differential escape of the intrinsic heat flux offsets the solar heating contrast and moist convection plays a key role. For Pegasi planets, such an offset between intrinsic and stellar fluxes cannot occur, because the intrinsic flux is 10^4 times less than the total flux. The fact that the day-night heating contrast occurs at hemispheric scale — and that the relevant dynamical length scales for Pegasi planets are also hemispheric (Section 4.1) — increases our confidence that simple analysis, focusing on the hemispheric-scale circulation, can provide insight.
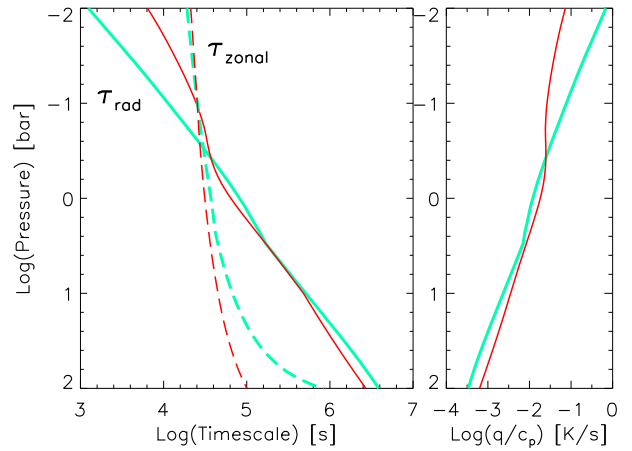

Fig. 4. *Left:* Characteristic time scales as a function of pressure level. τ_{zonal} is the minimal horizontal advection time (dashed). τ_{rad} is the timescale necessary to cool/heat a layer of pressure P and temperature T by radiation alone assuming the gas is optically thick (solid). (The plotted radiative timescale is an underestimate at pressures less than about 0.3 bars because the atmosphere becomes optically thin at those pressures.) For each case, the thin black and thick grey lines correspond to the hot and cold models from Section 2 and Fig.1. *Right:* Approximate cooling/heating rate as a function of pressure (see Eq. 18).

Because the Rossby number is small, the dominant balance in the horizontal momentum equation at mid-latitudes is between the Coriolis force and the pressure-gradient force (geostrophic balance). We adopt the primitive equations, which are the standard set of large-scale dynamical equations in a stably-stratified planetary atmosphere. When differentiated with pressure (which is used here as a vertical coordinate), this balance leads to the well-known thermal wind equation (e.g. Holton 1992, p. 75):

$$f\frac{\partial \mathbf{v}}{\partial \ln p} = -\mathcal{R}\mathbf{k} \times \nabla_{\mathbf{H}}\mathbf{T} \qquad (12)$$

where $\mathbf{v}$ is the horizontal wind, p is pressure, ∇_H is the horizontal gradient, T is temperature, and $\mathbf{k}$ is the unit upward vector. Assuming the interior winds are small

compared to the atmospheric winds, this implies that, to order-of-magnitude,

$$|\mathbf{v}| \sim \frac{\mathcal{R}}{fR}\Delta T_{\mathrm{horiz}}\Delta \ln p \tag{13}$$

where $|\mathbf{v}|$ and $\Delta T_{\mathrm{horiz}}$ are the characteristic wind speed and horizontal temperature difference in the atmosphere and $\Delta \ln p$ is the difference in log-pressures from bottom to top of the atmosphere. Non-sychronous rotation of the interior would alter the relation by changing the value of f, but the uncertainty from this source is probably a factor of two or less (see Eq. (6) and subsequent discussion).

The thermodynamic energy equation is, using pressure as a vertical coordinate (e.g. Holton 1992, p. 60),

$$\frac{\partial T}{\partial t} + \mathbf{v}\cdot\nabla_{\mathrm{H}}T - \omega\frac{H^2 N^2}{\mathcal{R}p} = \frac{q}{c_p} \tag{14}$$

where t is time, $\omega = dp/dt$ is vertical velocity, q is the specific heating rate (erg $\mathrm{g}^{-1}\,\mathrm{sec}^{-1}$), and we have assumed an ideal gas.

A priori, it is unclear whether the radiative heating and cooling is dominantly balanced by horizontal advection (second term on left of Eq. (14)) or vertical advection (third term on the left). To illustrate the possibilities, we consider two endpoint scenarios corresponding to the two limits. In the first scenario, the radiation is balanced purely by horizontal advection: zonal winds transport heat from dayside to nightside, and meridional winds transport heat from equator to pole. In the second scenario, the radiation is balanced by vertical advection (ascent on dayside, descent on nightside).

Consider the first scenario, where horizontal advection dominates. Generally, we expect $\mathbf{v}$ and $\nabla_{\mathrm{H}}T$ to point in different directions, so to order of magnitude their dot product equals the product of their magnitudes. (If the direction of $\nabla_{\mathrm{H}}T$ is independent of height and no deep barotropic flow exists, then at mid-latitudes one could argue that winds and horizontal pressure gradients are perpendicular to order Ro. However, the existence of either asynchronous rotation or variations in the orientations of $\nabla_{\mathrm{H}}T$ with height will imply that winds and $\nabla_{\mathrm{H}}T$ are not perpendicular even if $Ro << 1$. Because asynchronous rotation and variation in the directions of $\nabla_{\mathrm{H}}T$ with height are likely, and because, in any case, $\mathbf{v}$ and $\nabla_{\mathrm{H}}T$ will not be perpendicular near the equator, we write the dot product as the product of the magnitudes.) An order-of-magnitude form of the energy equation is then

$$\frac{|\mathbf{v}|\Delta T_{\mathrm{horiz}}}{R} \sim \frac{q}{c_p} \tag{15}$$

The solutions are

$$|\mathbf{v}| \sim \left(\frac{q}{c_p}\frac{\mathcal{R}\Delta \ln p}{f}\right)^{1/2} \tag{16}$$

$$\Delta T_{\mathrm{horiz}} \sim R\left(\frac{q}{c_p}\frac{f}{\mathcal{R}\Delta \ln p}\right)^{1/2} \tag{17}$$

A rough estimate of the heating rate, q/c_p, results from the analysis in Section 4.1:

$$\frac{q}{c_p} = \frac{4\sigma T^3 \Delta T g}{pc_p} \tag{18}$$

where ΔT is the characteristic magnitude of the difference between the actual and radiative equilibrium temperatures in the atmosphere. The heating rate depends on the dynamics through ΔT. We simply evaluate the heating rate using Eq. (18) with $\Delta T \approx T/2$. The results are shown in Fig. 4.

The key difficulty in applying the equations to Pegasi planets is the fact that q/c_p depends on pressure, and $\Delta T_{\mathrm{horiz}}$ probably should too, but Eqs. (16) and (17) were derived assuming that $\Delta T_{\mathrm{horiz}}$ is constant. We can still obtain rough estimates by inserting values of q/c_p at several pressures. At $\sim$ 50–100 bars, where $q/c_p \sim 10^{-4}$–$10^{-3}\,\mathrm{K\,sec}^{-1}$, we obtain temperature differences and wind speeds of 50–150 K and 200–600 $\mathrm{m\,sec}^{-1}$. At 1 bar, where q/c_p reaches $10^{-2}\,\mathrm{K\,sec}^{-1}$, the estimated temperature contrast and wind speed is $\sim$ 500 K and $\sim$ 2000 $\mathrm{m\,sec}^{-1}$. The estimates all assume $f \approx 3 \times 10^{-5}\,\mathrm{sec}^{-1}$, $\mathcal{R} = 3500\,\mathrm{J\,kg\,K}^{-1}$, and $\Delta \ln p \approx 3$.

Later we show that the equations successfully predict the mean wind speeds and temperature differences obtained in numerical simulations of the circulation of HD209458b. This gives us confidence in the results.

Now consider the second scenario, where vertical advection (third term on the left of Eq. (14)) balances the radiative heating and cooling. The magnitude of ω can be estimated from the continuity equation. Purely geostrophic flow has zero horizontal divergence, so ω is roughly

$$\omega \sim Ro\frac{|\mathbf{v}|}{R}p \tag{19}$$

Strictly speaking, this is an upper limit, because the non-linear terms comprising the numerator of the Rossby number contain some terms (e.g., the centripetal acceleration) that are divergence-free. Substituting this expression into the energy equation, using Eq. (13), and setting $Ro = |\mathbf{v}|/fR$ implies that

$$|\mathbf{v}| \sim \frac{R}{NH}\left(\frac{q}{c_p}f\mathcal{R}\right)^{1/2} \tag{20}$$

$$\Delta T_{\mathrm{horiz}} \sim \frac{fR^2}{NH\Delta \ln p}\left(\frac{q}{c_p}\frac{f}{\mathcal{R}}\right)^{1/2} \tag{21}$$

Numerical estimates using $H = 700\,\mathrm{km}$, $N \sim 0.0015\,\mathrm{sec}^{-1}$, and $q/c_p = 10^{-4}$–$10^{-3}\,\mathrm{K\,sec}^{-1}$ (appropriate to 50–100 bars) yield temperature differences and speeds of 80–250 K and 300–900 $\mathrm{m\,sec}^{-1}$, respectively. Here we

have used the same values for R and f as before. A heating rate of $10^{-2}\,\mathrm{K\,sec^{-1}}$, appropriate at the 1 bar level, yields $|\mathbf{v}| \sim 3000\,\mathrm{m\,sec^{-1}}$ and $\Delta T_{\mathrm{horiz}} \sim 800\,\mathrm{K}$. These values are similar to those obtained when we balanced heating solely against horizontal advection.

We can estimate the vertical velocity under the assumption that vertical advection balances the heating. Expressing the vertical velocity w as the time derivative of an air parcel's altitude, and using $w = -\omega/\rho g$, where ρ is density, yields

$$w \sim \frac{q}{c_p}\frac{\mathcal{R}}{HN^2} \tag{22}$$

Using $q/c_p = 10^{-2}\,\mathrm{K\,sec^{-1}}$ and $H = 700\,\mathrm{km}$ implies that $w \sim 20\,\mathrm{m\,sec^{-1}}$ near 1 bar. If this motion comprises the vertical branch of an overturning circulation that extends vertically over a scale height and horizontally over $\sim 10^{10}$ cm (a planetary radius), the implied horizontal speed required to satisfy continuity is $\sim 3000\,\mathrm{m\,sec^{-1}}$, consistent with earlier estimates.

The numerical estimates, while rough, suggest that winds could approach the upper limit of $\sim 3000\,\mathrm{m\,sec^{-1}}$ implied by the shear instability criterion. This comparison suggests that Kelvin-Helmholtz shear instabilities may play an important role in the dynamics.

The likelihood of strong temperature contrasts can also be seen from energetic considerations. The differential stellar heating produces available potential energy (i.e., potential energy that can be converted to kinetic energy through rearrangement of the fluid; Peixoto and Oort 1992, pp. 365-370), and in steady-state, this potential energy must be converted to kinetic energy at the rate it is produced. This requires pressure gradients, which only exist in the presence of lateral thermal gradients. A crude estimate suggests that the rate of change of the difference in gravitational potential Φ between the dayside and nightside on isobars caused by the heating is $\sim \mathcal{R}(q/c_p)\Delta \ln p$. The rate per mass at which potential energy is converted to kinetic energy by pressure-gradient work is $\mathbf{v} \cdot \nabla_H \Phi$, which is approximately $|\mathbf{v}|\mathcal{R}\Delta T_{\mathrm{horiz}}\Delta \ln p/R$. Equating the two expressions suggests, crudely, that $\Delta T_{\mathrm{horiz}} \sim (q/c_p)(R/|\mathbf{v}|)$, which implies $\Delta T_{\mathrm{horiz}} \sim 500\,\mathrm{K}$ using the values of q/c_p and $|\mathbf{v}|$ near 1 bar discussed earlier.

One could wonder whether a possible flow geometry consists of dayside upwelling, nightside downwelling, and simple acceleration of the flow from dayside to nightside elsewhere (leading to a flow symmetrical about the subsolar point). The low-Rossby-number considerations described above argue against this scenario. A major component of the flow must be perpendicular to horizontal pressure gradients. Direct acceleration of wind from dayside to nightside is still possible near the equator, however. This would essentially be an equatorially-confined Walker-type circulation that, as described earlier, would

lie equatorward of the geostrophic flows that exist at more poleward latitudes.

4.3. Numerical Simulations of the Circulation

To better constrain the nature of the circulation, we performed preliminary three-dimensional, fully-nonlinear numerical simulations of the atmospheric circulation of HD209458b. For the calculations, we used the Explicit Planetary Isentropic Coordinate, or EPIC, model (Dowling et al. 1998). The model solves the primitive equations in spherical geometry using finite-difference methods and isentropic vertical coordinates. The equations are valid in stably-stratified atmospheres, and we solved the equations within the radiative layer from 0.01 to 100 bars assuming the planet's interior is in synchronous rotation with the 3.5-day orbital period. The radius, surface gravity, and rotation rate of HD209458b were used ($10^8\,\mathrm{m}$, $10\,\mathrm{m\,sec^{-2}}$, and $\Omega = 2.1 \times 10^{-5}\,\mathrm{sec^{-1}}$, respectively).

The intense insolation was parameterized with a simple Newtonian heating scheme, which relaxes the temperature toward an assumed radiative-equilibrium temperature profile. The chosen radiative-equilibrium temperature profile was hottest at the substellar point (0° latitude, 0° longitude) and decreased toward the nightside. At the substellar point, the profile's height-dependence was isothermal at 550 K at pressures less than 0.03 bars and had constant Brunt-Vaisala frequency of $0.003\,\mathrm{sec^{-1}}$ at pressures exceeding 0.03 bars, implying that the temperature increased with depth. The nightside radiative-equilibrium temperature profile was equal to the substellar profile minus 100 K; it is this day-night difference that drives all the dynamics in the simulation. The nightside profile was constant across the nightside, and the dayside profile varied as

$$T_{\mathrm{dayside}} = T_{\mathrm{nightside}} + \Delta T_{\mathrm{rad}} \cos \alpha \tag{23}$$

where T_{dayside} is the dayside radiative-equilibrium temperature at a given latitude and longitude, $T_{\mathrm{nightside}}$ is the nightside radiative-equilibrium temperature, $\Delta T_{\mathrm{rad}} = 100\,\mathrm{K}$, and α is the angle between local vertical and the line-of-sight to the star. For simplicity, the timescale over which the temperature relaxes to the radiative-equilibrium temperature was assumed constant with depth with a value of 3×10^5 sec. This is equal to the expected radiative timescale at a pressure of about 5 bars (Fig. 4, left).

The Newtonian heating scheme described above is, of course, a simplification. The day-night difference in radiative-equilibrium temperature, 100 K, is smaller than the expected value. Furthermore, the radiative timescale is too long in the upper troposphere (~ 0.1–1 bar) and too short at deeper pressures of ~ 10–100 bars. Nevertheless, the net column-integrated heating per area produced by the scheme ($\mathrm{W\,m^{-2}}$) is similar to that expected to occur in the deep troposphere of HD209458b and other Pegasi

planets, and the simulation provides insight into the circulation patterns that can be expected.

The temperature used as the initial condition was isothermal at 500 K at pressures less than 0.03 bars and had a constant Brunt-Vaisala frequency of $0.003\,\mathrm{sec}^{-1}$ at pressures exceeding 0.03 bars. There were no initial winds. The simulations were performed with a horizontal resolution of 64×32 with 10 layers evenly spaced in log-pressure.

Figure 5–8 show the results of such a simulation. Despite the motionless initial condition, winds rapidly develop in response to the day-night heating contrast, reaching an approximate steady state after ~ 400 Earth days. Snapshots at 42 and 466 days are shown in Figs. 5 and 6, respectively. In these figures, each panel shows pressure on an isentrope (greyscale) and winds (vectors) for three of the model layers corresponding to mean pressures of roughly 0.4, 6, and 100 bars (top to bottom, respectively). The greyscale is such that, on an isobar, light regions are hot and dark regions are cold.

The simulation exhibits several interesting features. First, peak winds exceed $1\,\mathrm{km\,sec}^{-1}$, but despite these winds, a horizontal temperature contrast is maintained. The dayside (longitudes $-90°$ to $90°$) is on average hotter than the nightside, but dynamics distorts the temperature pattern in a complicated manner. Second, an equatorial jet develops that contains most of the kinetic energy. The jet initially exhibits both eastward and westward branches (Fig. 5) but eventually becomes only eastward (Fig. 6), and extends from $-30°$ to $30°$ in latitude. Third, away from the equator, winds develop that tend to skirt parallel to the temperature contours. This is an indication that geostrophic balance holds. (Because the thermal structure is independent of height to zeroeth order and we have assumed no deep barotropic flow, horizontal pressure and temperature gradients are parallel.) Nevertheless, winds are able to cross isotherms near the equator, and this is important in setting the day-night temperature contrast. As expected from the order-of-magnitude arguments in Section 4.1, the jets and gyres that exist are broad in scale, with a characteristic width of the planetary radius.

In the simulation, the day-night temperature difference (measured on isobars) is about 50 K. This value depends on the adopted heating rate, which was chosen to be appropriate to the region where the pressure is tens of bars. Simulations that accurately predict the day-night temperature difference at 1 bar will require a more realistic heating-rate scheme; we will present such simulations in a future paper.

The temperature patterns in Figs. 5 and 6 show that Earth-based infrared measurements can shed light on the circulation of Pegasi planets. In Fig. 6, the superrotating equatorial jet blows the high-temperature region downwind. The highest-temperature region is thus *not* at the substellar point but lies eastward by about 60° in longitude. The maximum and minimum temperatures would thus face Earth *before* the transit of the planet behind
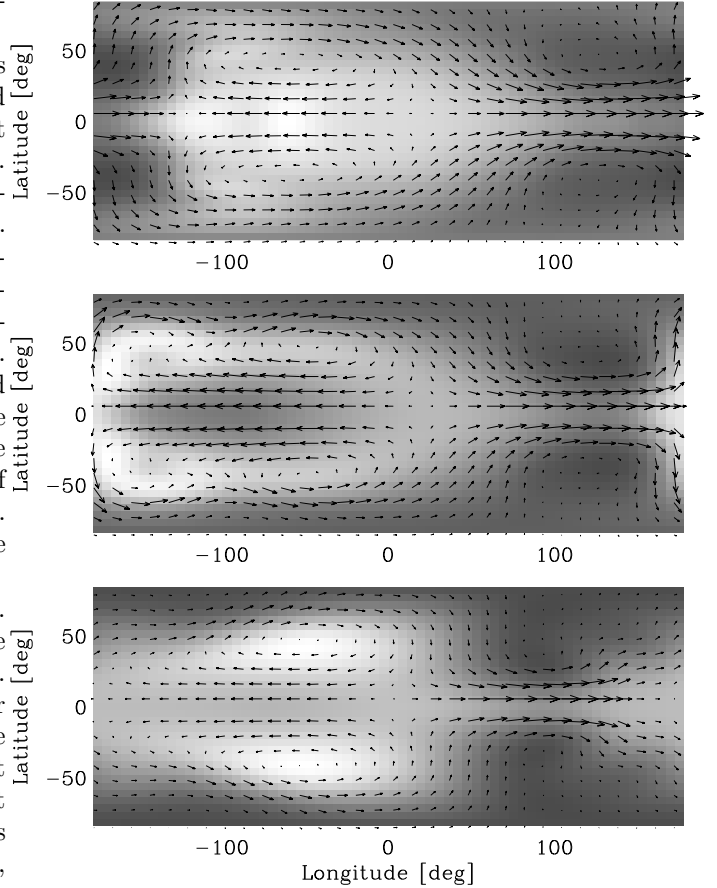

Fig. 5. EPIC simulation of atmospheric circulation on HD209458b after 42 days. Panels depict pressure on an isentrope (greyscale) and winds (vectors) for three model levels with mean pressures near 0.4, 6, and 100 bars (top to bottom, respectively). From top to bottom, the maximum wind speeds are 937, 688, and $224\,\mathrm{m\,sec}^{-1}$, respectively, and the greyscales span (from dark to white) 0.31–0.49 bars, 5.6–7.8 bars, and 92–113 bars, respectively. Substellar point is at 0° latitude, 0° longitude.

and in front of the star, respectively. On the other hand, if a broad westward jet existed instead, the maximum and minimum temperatures would face Earth *after* the transits. Therefore, an infrared lightcurve of the planet throughout its orbital cycle would help determine the direction and strength of the atmospheric winds.

In the simulation, the intense heating and cooling causes air to change entropy and leads to vertical motion, as shown in Fig. 7. Light regions (Fig. 7) indicate heating, which causes ascent, and dark regions indicate cooling, which causes descent. Air is thus exchanged between model layers. This exchange also occurs across the model's lowermost isentrope, which separates the radiative layer from the convective interior (Fig. 7, bottom). Because upgoing and downgoing air generally have different kinetic energies and momenta, energy and momentum
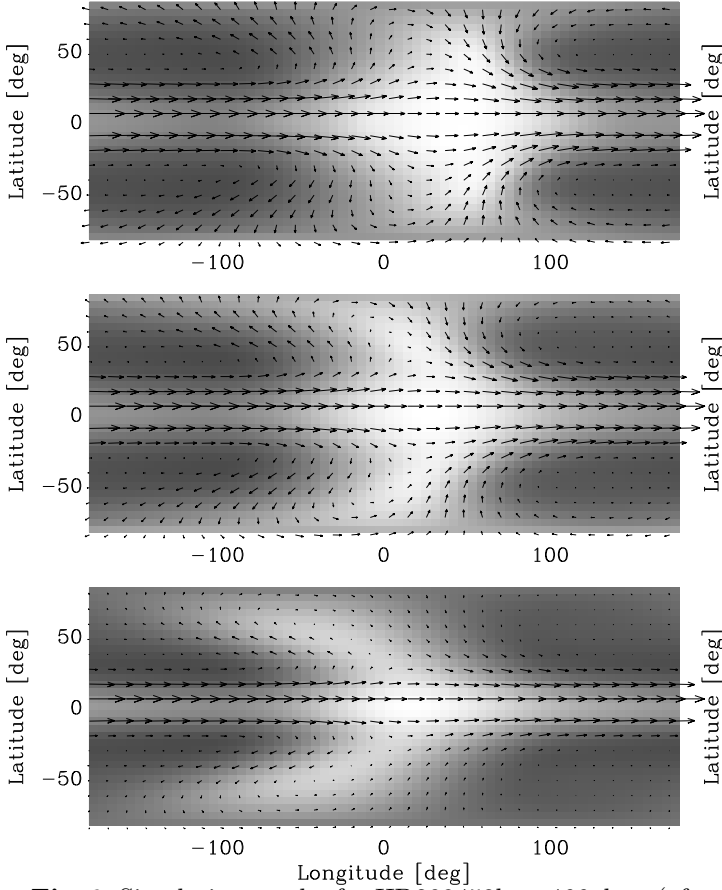
Fig. 6. Simulation results for HD209458b at 466 days (after a steady state has been reached). As in Fig. 5, panels depict pressure on isentropes (greyscale) and winds (vectors) for three model levels with mean pressures near 0.4, 6, and 100 bars (top to bottom, respectively). From top to bottom, the maximum wind speeds are 1541, 1223, and 598 m sec^{-1}, respectively, and the greyscales span (from dark to white) 0.32–0.51 bars, 5.6–8.1 bars, and 90–127 bars, respectively. Substellar point is at 0° latitude, 0° longitude.
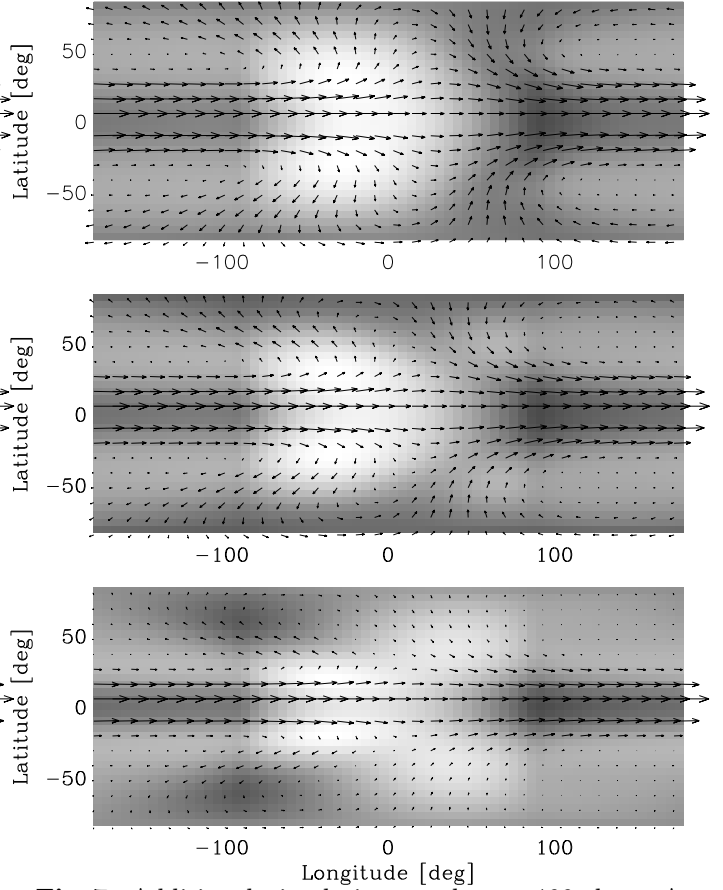
Fig. 7. Additional simulation results at 466 days. Arrows are identical to those in Fig. 6, but here greyscale is vertical velocity $d\theta/dt$, where θ is potential temperature. Light regions are heating (i.e., θ is increasing) and dark regions are cooling (θ is decreasing). From top to bottom, the greyscales span (from dark to white) -0.003 to $0.003 \, \mathrm{K\, sec^{-1}}$, -0.002 to $0.002 \, \mathrm{K\, sec^{-1}}$, and -0.001 to $0.001 \, \mathrm{K\, sec^{-1}}$, respectively. The lowermost panel separates the convective interior from the radiative region, and the implication is that mass exchange can happen across this interface.

can thus be exchanged between the atmosphere and interior.

Figure 8 indicates how the steady state is achieved. The build-up of the mass-weighted mean speed (top panel) involves two timescales. Over the first 10 days, the mean winds accelerate to 110 m sec^{-1}, and the peak speeds approach 1 km sec^{-1}. This is the timescale for pressure gradients to accelerate the winds and force balances to be established. The flow then undergoes an additional, slower (~ 300 day) increase in mean speed to 300 m sec^{-1}, with peak speeds of ~ 1.5 km sec^{-1}. This timescale is that for exchange of momentum with the interior, across the model's lowermost isentrope, to reach steady state, as shown in Fig. 8, middle.

In the simulation, kinetic energy is transported from the atmosphere into the interior at a rate that reaches 2500 W m^{-2} (Fig. 8, bottom). This downward transport of kinetic energy is $\sim 1\%$ of the absorbed stellar flux and is great enough to affect the radius of HD209458b, as shown in Paper I. Although the simulation described here does not determine the kinetic energy's fate once it reaches the convective interior, we expect that tidal friction, Kelvin-Helmholtz instabilities, or other processes could convert these winds to thermal energy. The exact kinetic energy flux will depend on whether a deep barotropic flow exists. Furthermore, potential and thermal energy are also transported through the boundary, and pressure work is done across it. Our aim here is not to present detailed di-

agnostics of the energetics, but simply to point out that energy fluxes that are large enough to be important can occur. We are currently conducting more detailed simulations to determine the sensitivity of the simulations to a deep barotropic flow, and we will present the detailed energetics of these simulations in a future paper.

The evolution of angular momentum (Fig. 8, middle) helps explain why the circulation changes from Fig. 5 to 6. After 42 days (Fig. 5), eastward midlatitude winds have already developed that balance the negative equator-to-pole temperature gradient. But at this time, the atmosphere's angular momentum is still nearly zero relative to the synchronously-rotating state, so angular momentum balance requires westward winds along some parts of the equator. (Interestingly, in these regions, the temperature *increases* with latitude, as expected from geostrophy.) The circulation involves upwelling on the dayside and equatorial flow — both east and west — to the nightside, where downwelling occurs. This circulation is similar in some respects to the Walker circulation in Earth's atmosphere. After 466 days, however, the atmosphere has gained enough angular momentum that the equatorial jet is fully superrotating. Some westward winds exist at high latitudes, but they are weak enough that the net angular momentum is still eastward.

Application of the arguments from Section 4.2 provides a consistency check. The mean heating rate in the simulations is about $1.7 \times 10^{-4}\,\mathrm{K\,sec^{-1}}$. Inserting this value into Eqs. (16–17), we obtain $\Delta T_{\mathrm{horiz}} = 70\,\mathrm{K}$ and $|\mathbf{v}| = 240\,\mathrm{m\,sec^{-1}}$. These compare well with the day-night temperature difference and mass-weighted mean speed of $50\,\mathrm{K}$ and $300\,\mathrm{m\,sec^{-1}}$ that are obtained in the simulation. (For the estimate, we used $f = 3 \times 10^{-5}\,\mathrm{sec^{-1}}$, $\mathcal{R} = 3500\,\mathrm{J\,kg^{-1}\,K^{-1}}$, $R = 10^8\,\mathrm{m}$, and $\Delta p = 3$.) If Eqs. (20–21) are adopted instead, using values of $N = 0.003\,\mathrm{sec^{-1}}$ and $H = 300\,\mathrm{km}$, we obtain temperature differences and speeds of $130\,\mathrm{K}$ and $470\,\mathrm{m\,sec^{-1}}$. Compared to the simulation, these estimates are too high by a factor of ~ 2, but are still of the correct order of magnitude. An important point is that the *maximum* speed in the simulation substantially exceeds that from the simple estimates; the estimates are most relevant for the mean speed.

4.4. Vertical motion and clouds

As shown in the appendix, hot and cold regions on the planet may have distinct chemical equilibrium compositions. Advection of air between these regions plays a key role for the (disequilibrium) chemistry in the atmosphere. Cloud formation critically depends on whether vertical motions dominate over horizontal motions. This in turns affects the albedo and depth to which stellar light is absorbed.

Clouds form when the temperature of moving air parcels decreases enough for the vapor pressure of condensible vapors to become supersaturated. If dayside heat-
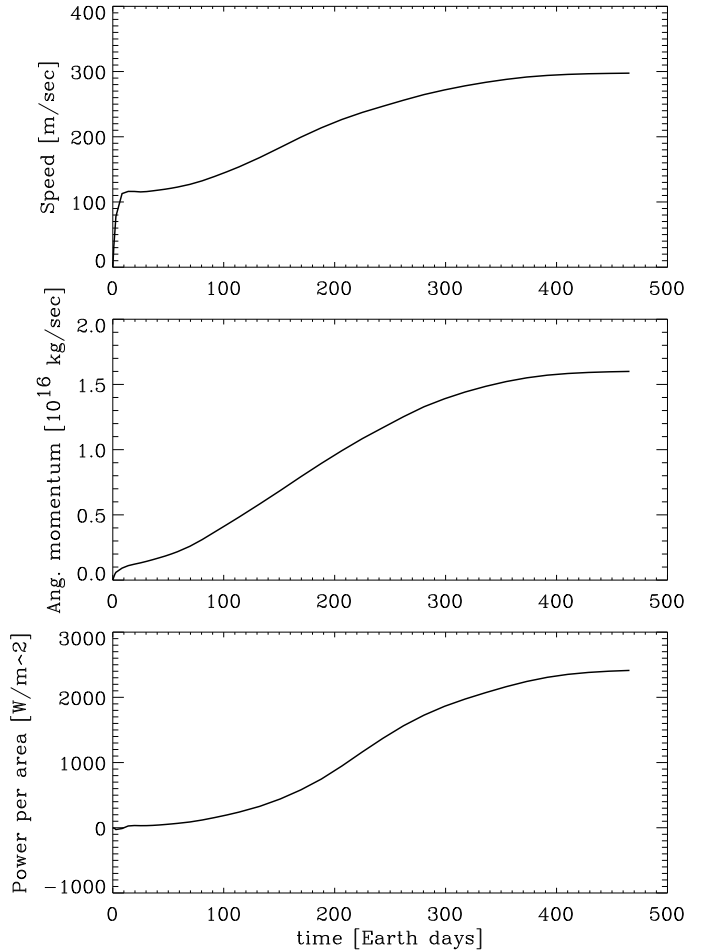

Fig. 8. *Top:* Mass-weighted mean wind speed within the model domain ($\sim$ 0.01–100 bar) during the simulation of HD209458b shown in Figs. 5–7. *Middle:* Globally-averaged zonal angular momentum per area minus that of the synchronously-rotating state. (That is, $RA^{-1}\int u\cos\phi\,dm$, where A is the planet's area, u is eastward speed, ϕ is latitude, and dm is an atmospheric mass element.) *Bottom:* Globally-averaged flux of kinetic energy across the model's bottom isentrope (at $\sim$ 100 bars), which is the interface between the radiative layer and the convective interior in this model.

ing and nightside cooling are balanced only by horizontal advection, air flowing from dayside to nightside remains at constant pressure but decreases in temperature (hence entropy) because of the radiative cooling. Nightside condensation may occur, and particle fallout limits the total mass of the trace constituent (vapor plus condensates) in this air. As the air flows onto the dayside, its temperature increases and any existing clouds will sublimate. This scenario therefore implies that the dayside will be cloud-free.

In an alternate scenario, dayside heating and nightside cooling are balanced by vertical advection, at least near the sub- and antisolar points. Because entropy increases

with altitude in a stably-stratified atmosphere, this scenario implies that ascent occurs on the dayside and descent on the nightside. Clouds may therefore form on the dayside, increasing the albedo and decreasing the pressure at which stellar light is absorbed.

In reality, both horizontal and vertical advection are important, and the real issue is to determine the relative contribution. We are pursuing more detailed numerical simulations to address this issue.

5. Conclusions

We examined the structure and dynamics of the atmospheres of Pegasi planets and concluded that strong day-night temperature contrasts (300 K or more) are likely to occur near the level where radiation is emitted to space ($\sim$ 1 bar). These temperature variations should drive a rapid circulation with peak winds of $1\,\mathrm{km\,sec^{-1}}$ or more. Force-balance arguments suggest that the mean midlatitude winds are eastward, but the equatorial winds could blow either east or west. Depending on the dynamical regime, the cloud coverage and consequently the radiative absorption of the incoming stellar flux will be very different.

Preliminary numerical simulations show that, while the dayside is generally hotter than the nightside, the specific temperature distribution depends on the dynamics. In our simulations, a broad superrotating jet develops that sweeps the high-temperature regions downwind by about 1 radian. This implies that the greatest infrared flux would reach Earth $\sim$ 10–15 hours before the occultation of the planet behind the star. On the other hand, if a subrotating jet existed, the greatest infrared flux would reach Earth *after* the occultation. Measurements of the infrared lightcurve of Pegasi planets will therefore constrain the direction and magnitude of the wind.

The simulations also produce a downward flux of kinetic energy across the $\sim$ 100 bar surface equal to $\sim$ 1% of the absorbed stellar flux. Although the simulation did not explicitly include the convective interior, we surmise that a substantial fraction of this kinetic energy would be converted to thermal energy by Kelvin-Helmholtz instabilities and other processes. As discussed in Paper I, "standard" evolution models explain HD209458b's radius only when the atmosphere is assumed to be unrealistically hot, but addition of an internal energy source allows a more realistic model to match the observed radius. The downward transport and subsequent dissipation of kinetic energy described here is a promising candidate. Bodenheimer et al. (2001) suggested an alternative — that the internal heating could be provided by tidal circularization of an initially eccentric orbit. The difficulty, as Bodenheimer et al. were careful to point out, is that the tidal heating is a transient process in the absence of a detected close, massive companion capable of exciting the planet's eccentricity. In contrast, the mechanism proposed here can

last throughout the star's lifetime. Nevertheless, to fully determine the feasibility of the mechanism, more detailed numerical simulations are required (in particular, to test the dependence of the energetics on the possible existence of winds in the interior). We will present such simulations in a future paper.

Upcoming observations are likely to provide key information within the decade. Several spacecraft missions (either proposed or accepted) and dedicated ground programs will observe extrasolar planets. Measurement of starlight reflected from these planets may allow the albedo to be estimated. Because the star-planet-Earth angle changes throughout the planet's orbit, crude information on the scattering properties of the atmosphere (e.g., isotropic versus forward scattering) may be obtainable. Asymmetries in the reflected flux as the planet approaches and recedes from the transit could give information on the differences of albedo near the leading and trailing terminators, which would help constrain the dynamics. Finally, transit observations of Pegasi planets using high resolution spectroscopy should in the near future yield constraints on the atmospheric temperature, cloud/haze abundance, and winds (Brown 2001; see also Seager & Sasselov 2000; Hubbard et al. 2001). If these measurements are possible during the ingress and egress, i.e., the phases during which the planets enters and leaves the stellar limb, respectively, asymmetries of the planetary signal should be expected and would indicate zonal heat advection at the terminator. The duration of these phases being limited to less than 10 minutes, it is not clear that this effect is observable with current instruments.

Appendix A: Day-night temperature variations and chemical composition

Here we explore the implications of day-night temperature variations on the abundances of a condensing species. Suppose that on the day side, a given condensate (e.g. iron) condenses at a pressure level $P^\star_{\mathrm{day}}$ and a corresponding temperature T_{day}. If the temperature on the night side T_{night} is smaller, at what pressure $P^\star_{\mathrm{night}}$ will condensation take place?

Assuming an ideal gas, we write the Clausius-Clapeyron equation as

$$\frac{d\ln p}{d\ln T} = \beta \tag{A.1}$$

where p is the partial pressure of saturation of the condensing species and $\beta = L/\mathcal{R}T$ is the ratio of the latent

heat of condensation L to the thermal energy $\mathcal{R}T$. For most condensing species of significance here, $\beta \approx 10$. We furthermore assume that β is independent of T and P, which introduces only a slight error in our estimates.

By definition, on the day side, the saturation abundance of the condensing species, $x = p/P$ is maximal and equal to $x^\star$ at $P = P_{\mathrm{day}}^\star$. On the other hand, the night side temperature is lower and the abundance becomes:

$$\ln x(P_{\mathrm{day}}^\star) = \ln x^\star - \beta \ln(T_{\mathrm{day}}/T_{\mathrm{night}}). \tag{A.2}$$

In order to reach condensation, i.e. $x = x^\star$, one has to penetrate deeper into the atmosphere. Eq. (A.1) implies that

$$\frac{d \ln x}{d \ln P} = \beta \nabla_T - 1, \tag{A.3}$$

and hence, on the night side,

$$\ln x(P) = \ln x(P_{\mathrm{day}}^\star) + (\beta \nabla_T - 1) \ln(P/P_{\mathrm{day}}^\star), \tag{A.4}$$

assuming that ∇_T is constant. Using eq. (A.2), one obtains the condensation pressure on the night side:

$$\frac{P_{\mathrm{night}}^\star}{P_{\mathrm{day}}^\star} = \left(\frac{T_{\mathrm{day}}}{T_{\mathrm{night}}} \right)^{\beta/(\beta \nabla_T - 1)}. \tag{A.5}$$

Using $\beta \sim 10$, $\nabla_T \sim 0.15$ and $T_{\mathrm{day}}/T_{\mathrm{night}} \sim 1.2$, one finds $P_{\mathrm{night}}^\star \sim 38 P_{\mathrm{day}}^\star$, a very significant variation of the condensation pressure. This implies that air flowing on constant pressure levels around the planet would lead to a rapid depletion of any condensing species on the day side, compared to what would be predicted from chemical equilibrium calculations. This can potentially also remove important absorbing gases from the day side, as in the case of TiO, which can be removed by $CaTiO_3$ condensation, or Na, removed by Na_2S condensation (Lodders 1999). Of course, most of the variation depends on the exponential factor $\beta/(\beta \nabla_T - 1)$, which is infinite in the limit when the atmospheric temperature profile and the condensation profile are parallel to each other.

In the discussion, we implicitly assumed $\beta \nabla_T - 1 > 0$; however, when the atmosphere is close to an isotherm, this factor can become negative. In this case the day/night effect is even more severe, as the condensing species is entirely removed from this quasi-isothermal region.

References

Allard F., Hauschildt P.H., Alexander D.R., Starrfield S. 1997, ARA&A, 35, 137

Andrews D.G., Holton J.R., Leovy C.B., 1987, *Middle Atmosphere Dynamics* Academic Press, New York

Banfield, D., Murray, N. 1992, Icarus, 99, 390

Barman T., Hauschildt P.H., Allard F. 2001, ApJ, 556, 885

Bodenheimer P., Lin D.N.C., Mardling R. 2001, ApJ, 548, 466

Brown T.M. 2001, ApJ, 553, 1006

Burrows A., Guillot T., Hubbard W.B., Marley M.S., Saumon D., Lunine J.I., Sudarsky D. 2000, ApJL, 534, L97

Burrows, A., Marley, M., Hubbard, W.B., Lunine, J.I., Guillot, T., Saumon, D., Freedman, R., Sudarsky, D., Sharp, C., 1997, ApJ, 491, 856.

Chandrasekhar, S. 1961, Hydrodynamic and Hydromagnetic Stability, Clarendon Press, Oxford, p. 491

Charbonneau D., Brown T.M., Latham D.W., Mayor, M., 2000, ApJ 529, L45

Cho J.Y-K., Polvani L.M., 1996, Science 273, 335

Dermott, S.F. Icarus, 37, 310

Dowling, T.E., Fischer, A.S., Gierasch, P.J., Harrington, J., LeBeau, R.P. Jr., Santori, C.M., 1998, Icarus 132, 221

Geballe T.R., Saumon D., Leggett S.K., Knapp G.R., Marley M.S., Lodders K. 2001, ApJ, 556, 373

Gill A.E., 1982, *Atmosphere-Ocean Dynamics* Academic Press, New York

Gold T., Soter S. 1969, Icarus, 11, 356.

Goldreich P., Soter S. 1966, Icarus, 5, 375

Goukenleuque C., Bézard B., Joguet B., Lellouch E., Freedman R., 2000, Icarus 143, 308

Guillot T., Showman A.P. 2001, submitted to A&A (Paper I)

Guillot T., Burrows A., Hubbard W.B., Lunine J.I., Saumon D., 1996, ApJ 459, L35

Henry G.W., Marcy G.W., Butler R.P., Vogt, S.S., 2000, ApJ 529, L41-L44

Holton J.R., 1992, *An Introduction to Dynamic Meteorology*, Academic Press, New York.

Houben H., Young R.E., Showman A., Mosqueira I. 2001, *Jupiter: Planet, Satellites, & Magnetosphere* [abstract for conference held in Boulder, CO, June 25-30 2001], 51.

Hubbard W.B. 1984. Planetary Interiors. New York: Van Nostrand Reinhold Co., Inc.

Hubbard W.B., Fortney J.J., Lunine J.I., Burrows A., Sudarsky D., Pinto P.A. 2001, submitted to ApJ

Ingersoll A.P., Barnet C.D., Beebe R.F. et al., 1995, in: Neptune and Triton, ed. D.P. Cruikshank, University of Arizona Press, Tucson, 613

Ingersoll A.P., Dobrovolskis A.R., 1978, Nature 275, 37

Ioannou P.J., Lindzen R.S. 1993, ApJ, 406, 266

Liebert J., Reid I.N., Burrows A., Burgasser A.J., Kirkpatrick J.D., Gizis J.E. 2000, ApJL 533, L155

Lodders K. 1999, ApJ, 519, 793

Lubow S.H., Tout C.A., Livio M. 1997, ApJ, 484, 866

Maeder A., 1995, A&A, 299, 84

Marcy G.W., Butler R.P., Williams E., Bildsten L., Graham J.R., Ghez A.M., Jernigan J.G., 1997, ApJ, 481, 926

Marley M.S., Saumon D., Guillot T., et al., 1996, Science 272, 1919

Peale S.J., 1999, *Ann. Rev. Astron. Astrophys.*, 37, 533

Peixoto J.P., Oort A.H., 1992, *Physics of Climate,* American Institute of Physics, New York.

Rhines P.B., 1975, *J. Fluid. Mech.* 69, 417

Schweitzer A., Gizis J.E., Hauschildt P.H., Allard F., Reid I.N. 2001, ApJ, 555, 368

Seager S., Sasselov D.D., 1998, ApJ 502, L157

Seager S., Sasselov D.D. 2000, ApJ, 537, 916

Tittemore, W.C., Wisdom, J. 1989, Icarus, 78, 63

Zahn J.-P., 1992, A&A, 265, 115